



King's Research Portal

DOI:
[10.1002/mrm.27540](https://doi.org/10.1002/mrm.27540)

Document Version
Peer reviewed version

[Link to publication record in King's Research Portal](#)

Citation for published version (APA):

Roccia, E., Vidya Shankar, R., Neji, R., Lima da Cruz, G., Munoz, C., Botnar, R., Goh, V., Prieto, C., & Dregely, I. (2019). Accelerated 3D T₂ mapping with dictionary-based matching for prostate imaging. *Magnetic resonance in medicine*, 81(3), 1795-1805. <https://doi.org/10.1002/mrm.27540>

Citing this paper

Please note that where the full-text provided on King's Research Portal is the Author Accepted Manuscript or Post-Print version this may differ from the final Published version. If citing, it is advised that you check and use the publisher's definitive version for pagination, volume/issue, and date of publication details. And where the final published version is provided on the Research Portal, if citing you are again advised to check the publisher's website for any subsequent corrections.

General rights

Copyright and moral rights for the publications made accessible in the Research Portal are retained by the authors and/or other copyright owners and it is a condition of accessing publications that users recognize and abide by the legal requirements associated with these rights.

- Users may download and print one copy of any publication from the Research Portal for the purpose of private study or research.
- You may not further distribute the material or use it for any profit-making activity or commercial gain
- You may freely distribute the URL identifying the publication in the Research Portal

Take down policy

If you believe that this document breaches copyright please contact librarypure@kcl.ac.uk providing details, and we will remove access to the work immediately and investigate your claim.

Accelerated 3D T₂ Mapping with Dictionary-Based Matching for Prostate Imaging

Elisa Roccia¹, Rohini Vidya Shankar¹, Radhouene Neji^{1,2}, Gastão Cruz¹, Camila Munoz¹, René Botnar¹, Vicky Goh³, Claudia Prieto¹, and Isabel Dregely¹

¹ School of Biomedical Engineering and Imaging Sciences, King's College London, London, United Kingdom

² Siemens Healthcare Limited, Frimley, United Kingdom

³ Cancer Imaging, King's College London, London, United Kingdom

Submitted as Full Paper to Magnetic Resonance in Medicine

Running Title: Accelerated 3D T₂ mapping for Prostate Imaging

Word count: 4462

Corresponding author

Elisa Roccia

Department of Biomedical Engineering, 3rd floor, Lambeth Wing

St Thomas' Hospital, Westminster Bridge Road, London SE1 7EH, United Kingdom

Email: elisa.roccia@kcl.ac.uk

Key words: prostate cancer imaging; quantitative MRI; T₂ mapping; 3T MRI

ABSTRACT

Purpose: To develop a fast and accurate method for 3D T_2 mapping of prostate cancer using undersampled acquisition and dictionary-based fitting.

Methods: 3D high-resolution T_2 -weighted images ($0.9 \times 0.9 \times 3 \text{ mm}^3$) were obtained with a multi-shot T_2 -prepared balanced steady state free precession ($T_2\text{prep-bSSFP}$) acquisition sequence using a 3D variable density undersampled Cartesian trajectory. Each T_2 -weighted image was reconstructed using Total Variation regularized SENSE. A flexible simulation framework based on extended phase graphs generated a dictionary of magnetization signals, which was customized to the proposed sequence. The dictionary was matched to the acquired T_2 -weighted images to retrieve quantitative T_2 values, which were then compared to gold standard spin echo acquisition values using monoexponential fitting. The proposed approach was validated in simulations and a T_1/T_2 phantom, and feasibility was tested in eight healthy subjects.

Results: The simulation analysis showed that the proposed T_2 mapping approach is robust to noise and typically observed T_1 variations. T_2 values obtained in the phantom with $T_2\text{prep-bSSFP}$ and the acquisition-specific dictionary-based matching were highly correlated with the gold standard spin echo method ($r = 0.99$). Further, no differences were observed with the accelerated acquisition compared to the fully sampled acquisition ($r = 0.99$). T_2 values obtained in prostate peripheral zone, central gland and muscle in healthy subjects (age 26 ± 6 years) were $97 \pm 14 \text{ ms}$, $76 \pm 7 \text{ ms}$ and $36 \pm 3 \text{ ms}$, respectively.

Conclusion: 3D quantitative T_2 mapping of the whole prostate can be achieved in 3 min.

Key words: prostate cancer imaging; quantitative MRI; T_2 mapping; 3T MRI

INTRODUCTION

Prostate cancer (PCa) is one of the most frequent types of cancer in men, with more than 164 000 estimated new cases in the USA in 2018 ³. The standard clinical routine for its diagnosis consists of the measurement of serum prostate-specific antigen, digital rectal examination and transrectal ultrasound-guided biopsy. However, these approaches may not accurately detect cancer or assess its aggressiveness. Thus, many cases of high-risk clinically significant PCa are missed and, on the other hand, for the case of low-risk PCa overtreatment and underuse of active surveillance in this patient group remain a significant clinical challenge ^{4,5}.

Multiparametric magnetic resonance imaging (mpMRI) of the prostate, which consists of the acquisition of 2D T₂-weighted (T_{2w}), diffusion-weighted and gadolinium-based dynamic contrast-enhanced images, has shown great potential for diagnosis of PCa, and has been shown to correlate with pathologic Gleason score ^{4,5}. Efforts for standardization have resulted in consensus guidelines for acquisition, analysis and reporting (PIRADS) ^{6,7}. In particular, high-resolution T_{2w} imaging depicts prostate anatomy and has the ability to detect and characterize lesions. According to PIRADS, T_{2w} MRI is the primary image contrast in the transition zone ⁷. Cancerous lesions appear hypointense on T_{2w} MRI. The current literature reports that sensitivity of mpMRI for PCa detection and diagnosis is high (range of sensitivity values reported: 58 – 95%) ^{6,8,9}, however low specificity has been reported in the detection of clinically significant cancers ⁶, and low sensitivity in the detection of small, intermediate grade lesions, and of cancers located in the apex ⁹. While 2D T_{2w} images are evaluated in a qualitative manner, quantitative MRI directly relates the MR signals to quantitative tissue features enabling consistent and reproducible assessment, and thus more reliable treatment decisions.

Quantitative 3D MRI has thus promise to improve diagnostic ability, in particular in follow-up (active surveillance) and longitudinal studies ¹⁰. Quantitative mapping of T₂ relaxation rate has shown promising results for PCa discrimination ^{11–13}. Low T₂ values were found to correlate well with the low citrate levels of cancerous tissue, which is characterized by low acinar structure ¹⁴. Nevertheless, quantitative T₂ mapping is not yet standard in clinical routine because of the long scan times required for the acquisition of multiple T₂ contrasts ⁷. Therefore, the clinical challenge is the development of an accurate and robust method for quantitative T₂ mapping, with 3D coverage, high resolution and signal-to-noise ratio (SNR), which can be performed in clinically acceptable scan times.

The gold standard T₂ mapping approach consists of a 2D multi-contrast scan in

which several spin-echo (SE) images are acquired at different echo times (TE) and are then fitted pixelwise to a monoexponential function that models the T_2 decay^{10,11}. As the single-echo SE acquisition has prohibitively long scan times and is prone to motion artifacts due to peristalsis or physiological bulk motion, several undersampled reconstruction approaches have been proposed to enable T_2 mapping in feasible scan times^{11,15–20}. However, the scan time is still too long, thus the acquisition is typically limited to 2D. Faster imaging involves turbo spin-echo (TSE) acquisition, which reduces the scan time by echo train sampling. However, the length of the echo train (“turbo factor”), and thus the scan time reduction, is associated with increased image blurring. Moreover, to acquire multi-contrast T_2w images for quantitative T_2 mapping, the scan time may again be still too long. In multi-echo sequences, the contribution of stimulated echoes in the multi-echo SE echo train results in a deviation of the signal from the assumption of monoexponential behavior and hence leads to inaccurate estimates²¹.

Improved accuracy in T_2 quantification can be achieved using simulation-based methods rather than the standard oversimplified monoexponential fit. These methods are characterized by more complex but accurate modeling of the effects of the pulse sequence on the magnetization. To retrieve quantitative T_2 values in each voxel, a matching process is performed between the measured signal and a dictionary (database) of magnetization signals, which are generated using either Bloch or extended phase graphs²² (EPG) simulations^{20,23}.

Alternative acquisition sequences for T_2 mapping have been investigated such as Carr-Purcell-Meiboom-Gill sequence¹², double-echo steady-state (DESS)²⁴, and triple echo steady-state²⁵. The balanced steady-state free precession (bSSFP) sequence has been often used to perform segmented acquisitions preceded by T_2 magnetization preparation, with promising results in T_2 quantitative parametric mapping in both cardiac^{26–31} and prostate^{32–34} applications. In general, magnetization preparation sequences are advantageous because of the flexibility to add the preparation of multiple contrasts, such as T_1 -preparation³⁵, T_2 -preparation (T_2 prep)^{36,37}, fat saturation, and combinations of these²⁶.

In this study, we sought to develop accurate and fast 3D T_2 mapping of the whole prostate. We propose the use of an accelerated 3D multi-shot T_2 prep-bSSFP acquisition sequence, combined with a Cartesian Acquisition with Spiral PRofile order (CASPR)³⁸ trajectory. This trajectory is advantageous as it is Cartesian, and therefore does not require computationally demanding gridding steps in the reconstruction, it is centric in k_y - k_z thus

enabling the immediate encoding of the contrast generated by the magnetization preparation pre-pulses, and is suitable for undersampling to reduce scan time. For T_2 mapping, we use a dictionary-based T_2 mapping method that is customized to the acquisition sequence and specified imaging parameters. First, the dictionary-based T_2 mapping method is validated in both simulations and a standardized T_1/T_2 phantom experiment. Then, the undersampled acquisition is validated in the phantom, and a feasibility study is performed in eight healthy subjects.

METHODS

The 3D images were acquired using a prototype segmented multi-shot T_2 prep-bSSFP sequence (shot length = TR), where each readout is preceded by an adiabatic T_2 prep module^{36,37}. In order to stabilize the readout magnetization, 14 ramp-up pulses with linearly increasing flip angles and alternating phase were added before each readout.³⁹ In each shot a fixed number of bSSFP signals, so called segments, were acquired at unique k_y - k_z positions forming a 3D CASPR trajectory³⁸. This trajectory was modified to achieve prospective undersampling using a variable density (VD) undersampling scheme, with a 25% fully sampled center region of the k-space and an undersampled periphery (Figure 1a). The variable density data was reconstructed with Total Variation regularized SENSE (TV-SENSE) reconstruction^{40,41}. The acquisition was repeated with different T_2 prep durations to obtain different T_2 contrasts.

A simulation framework based on the EPG formalism²² was implemented in MATLAB (Mathworks, Natick, MA) and included the following parameters: number, FA and phase of both bSSFP and ramp-up pulses; pulses and duration of T_2 prep module; duration of each shot (TR). This framework enabled evaluation of the acquisition-specific magnetization evolution and was used to: 1) optimize the T_2 prep-bSSFP sequence parameters for maximum SNR and tissue contrast while keeping the acquisition time short, 2) characterize the robustness of the acquisition scheme to T_1 and flip angle (FA) variations, and 3) implement the dictionary-based T_2 matching.

The multi-dimensional dictionary of signals was generated such that each dictionary entry reflects the signal evolution as a function of a given tissue type (with intrinsic T_1 and T_2 relaxation rates) and fixed extrinsic parameters (specific to the T_2 prep-bSSFP imaging sequence). Each dictionary entry was calculated as the average over the first readout segment in each shot, so as to reflect encoding of the contrast information in the centric trajectory acquisition (Figure 1), and was plotted as a function of the T_2 prep duration. The range of the simulated relaxation times was $T_1 = [1200, \dots, 2300]$ ms (steps of 10 ms) and $T_2 = [20, \dots, 250]$ ms (steps of 1 ms), which represent typical prostate tissue values. The generation of the dictionary (2530 entries) took 111 min with a non-optimized implementation on a single CPU, and it was generated only once as all the sequence parameters are fixed for the whole study.

In order to determine the quantitative T_2 values, both the precomputed dictionary of simulated signals and the experimental data were first normalized by the respective first data point, which corresponds to a T_2 prep duration of 0 ms. Then, matching was performed

for each voxel by minimizing the L_2 -norm of the differences between the experimental data and the precomputed dictionary of simulated signals, with an exhaustive search over all dictionary entries. Depending on how much T_1 variation is expected, the dictionary-based T_2 matching can be performed either with a fixed global T_1 value or with a voxel-specific T_1 . The latter requires the separate acquisition and incorporation of a T_1 map into the matching algorithm. In this study, a voxel-specific T_1 was used for the phantom because of the significant variation of T_1 values of the different tubes, whereas a fixed global T_1 value was used for the healthy subjects.

A phantom experiment was performed to validate the proposed dictionary-based T_2 mapping technique and the undersampled VD acquisition. Feasibility for prostate T_2 mapping was then tested in healthy subjects, following approval by the local institutional review board and informed consent. Both phantom and in-vivo experiments were performed on a 3T PET-MR scanner (Biograph mMR, Siemens Healthcare, Erlangen, Germany).

Simulations

T_1 and FA dependence

To characterize potential confounding influences on T_2 estimates by (unknown) T_1 and FA variations, the simulated signal intensity was analyzed as a function of T_1 and FA for a range of T_2 values. A further simulation was performed to assess the impact on the T_2 estimated using the proposed approach if a globally fixed (rather than voxel-based measured) T_1 was used, and if this introduces a bias in the T_2 estimation. The following T_2 prep durations were used to build the dictionary: 0, 45, 70, 90, 120, and 150 ms. Four different dictionary entries were simulated representing different tissue types, for all combinations of low $T_1^{\text{true}} = 1700$ ms, high $T_1^{\text{true}} = 2200$ ms, low $T_2^{\text{true}} = 50$ ms, high $T_2^{\text{true}} = 150$ ms, with the T_2 values chosen to represent cancerous and healthy tissue as an average of typically reported T_2 values at 3T in the prostate peripheral zone ^{11,42–44}. Each of these dictionary entries was then matched to the dictionary assuming a globally fixed T_1 different from the T_1^{true} , to characterize deviations of T_2 estimates as a function of T_1 variations.

SNR analysis

Monte Carlo simulations were performed to evaluate the robustness to noise of the proposed approach, compared to the reference monoexponential fitting. Different levels of random white Gaussian noise (SNR = 10, 20, 30, 40, 50, 80, 100) were added to the

simulated transverse magnetization for all the $T_{2\text{prep}}$, T_2 matching was performed, and this was repeated 5000 times. Accuracy and precision were then calculated as the mean and standard deviation of the T_2 values estimated over the 5000 repetitions, respectively. T_2 values were estimated using the dictionary matching with six different $T_{2\text{prep}}$ ($T_{2\text{prep}}$ duration: 0, 45, 70, 90, 120, 150 ms), with only three $T_{2\text{prep}}$ ($T_{2\text{prep}}$ duration: 0, 90, 150 ms), and also by using a simplified monoexponential fitting for comparison with the proposed dictionary-based matching. The SNR analysis was performed for two dictionary entries corresponding to different prostate tissue types: $T_1 = 2200$ ms⁴⁵ and $T_2^{\text{low/high}} = 50/150$ ms.

Phantom

Acquisition

A standard T_1/T_2 phantom, which contained 9 tubes with different T_1/T_2 relaxation times⁴⁶, was used to test the proposed T_2 mapping method. Imaging parameters of the proposed prototype 3D $T_{2\text{prep}}$ -bSSFP sequence were chosen according to EPG-guided sequence optimization, ensuring that the total acquisition time is minimized while maintaining SNR and contrast: shot length TR = 1600 ms, flip angle FA = 57°, number of bSSFP segments in each shot Nseg = 96, and 14 ramp-up pulses. Other imaging parameters were: transversal orientation, matrix size 304 x 304 x 32, resolution 0.9 x 0.9 x 3 mm³, and bSSFP-TR/TE = 4.0/2.0 ms. For T_2 mapping, three $T_{2\text{prep}}$ -bSSFP images with different $T_{2\text{prep}}$ durations (0, 90, 150 ms) were acquired sequentially, both fully sampled (FS) and VD. The choice of using only three $T_{2\text{prep}}$ durations was based on the simulation results, and on an additional experiment performed on the phantom which showed that the T_2 estimated with dictionary matching using three $T_{2\text{prep}}$ was highly correlated with values obtained using six $T_{2\text{prep}}$ (Supporting Information Figure S1). The acquisition time was TA = 2 min 40 s for a FS acquisition (100 shots) and 1 min for a VD factor of 3 (37 shots). For gold standard T_2 mapping, 2D single echo SE images with long TR (10 s) to allow for full magnetization recovery were also acquired, with TE matched to the three different $T_{2\text{prep}}$ durations. This was a single slice acquisition that matched the central slice of the 3D $T_{2\text{prep}}$ -bSSFP. Acquisition parameters for 2D SE were: matrix size 256 x 256, transversal orientation, resolution 1.17 x 1.17 mm², TR = 10 s, TEs = 12, 90, 150 ms, TA = 39 min for each T_{2w} image (total TA = 1 h 56 min). A single echo inversion recovery-SE (IR-SE) T_1 map was also acquired with matrix size 256 x 256, transversal

orientation, resolution $1.17 \times 1.17 \text{ mm}^2$, TR = 10 s (time between inversion pulses), TE = 12 ms, inversion time TI = 50, 100, 150, 300, 500, 1000, 2000, 4000, 6000 ms, TA = 43 min for each T_1 w image (total TA = 6 h 26 min).

Data analysis

The two sets (FS and VD) of three 3D T_2 prep-bSSFP T_2 w images were fitted to obtain quantitative T_2 maps in two ways: i) using a simple monoexponential model (which does not take into account incomplete magnetization recovery for a TR = 1600 ms), and ii) using the proposed approach with EPG-based dictionary matching. The reference standard SE T_2 map was obtained with a standard monoexponential fit. The IR-SE T_1 map was included in the matching algorithm to account for the significant variation of T_1 values of the different tubes. Regions of interest (ROIs) were drawn in the central slice of the 3D acquisition, which corresponds to the single slice of the 2D acquisition, for each phantom tube, and the T_2 estimates are presented as mean ROI value \pm standard deviation (STD). Particular attention was given to four phantom tubes characterized by different combinations of T_1 and T_2 relaxation times: low T_1 and T_2 (LL), low T_1 and high T_2 (LH), high T_1 and low T_2 (HL), and high T_1 and T_2 (HH).

The following comparisons were performed:

1. $SE^{\text{monoexponential}}$ vs $T_2\text{prep-bSSFP}_{FS}^{\text{monoexponential}}$ vs $T_2\text{prep-bSSFP}_{FS}^{\text{dictionary}}$: T_2 values obtained with gold standard 2D SE technique vs FS 3D T_2 prep-bSSFP using (simplified) monoexponential fit vs FS 3D T_2 prep-bSSFP using dictionary based-matching;
2. $T_2\text{prep-bSSFP}_{FS}^{\text{dictionary}}$ vs $T_2\text{prep-bSSFP}_{VD}^{\text{dictionary}}$: T_2 values obtained with FS vs VD 3D T_2 prep-bSSFP, both using dictionary-based matching;
3. $SE^{\text{monoexponential}}$ vs $T_2\text{prep-bSSFP}_{VD}^{\text{dictionary}}$: T_2 values obtained with gold standard 2D SE method (total TA = 1:56 hours) vs the proposed VD T_2 prep-bSSFP method (total TA = 3 min).

The results were compared using regression analysis and Pearson's correlation coefficient (r); statistical difference was tested using a paired-sample t test with threshold $P = 0.05$.

Healthy subjects

Acquisition

A feasibility study was performed and included eight healthy male subjects, age 26 ± 6 years. The in-vivo VD 3D T_2 prep-bSSFP acquisition parameters matched the phantom acquisition parameters: TR = 1600 ms, FA = 57° , Nseg = 96, transversal orientation, matrix size 304 x 304 x 32, resolution 0.9 x 0.9 x 3 mm³, bSSFP-TR/TE = 4.0/2.0 ms. Three T_2 prep durations (0, 90, 150 ms) were acquired sequentially. For image quality comparison purposes, a 2D transverse T_2 w TSE image (as standard in PIRADS mpMRI ⁷) was acquired for all eight subjects (320 x 256 matrix, 0.6 x 0.8 x 3 mm³ resolution, TR/TE = 6470/89 ms, FA = 150° , TA = 2 min 16 s), an example image is shown in Supporting Information Figure S2. To evaluate in-vivo scan/re-scan reproducibility, for one subject the three T_2 w images were acquired again with the proposed VD 3D T_2 prep-bSSFP protocol 9 months after the first scan.

Data analysis

The proposed dictionary-based T_2 mapping method with VD T_2 prep-bSSFP was applied to the whole healthy subject population. Based on our simulation results, a T_1 map was not included in the matching algorithm, but a fixed T_1 value of 2200 ms ⁴⁵ (representative of prostate T_1 at 3T) was used instead. In order to evaluate the impact of this choice on our results, a sensitivity experiment was performed in-vivo assuming different fixed T_1 in the dictionary matching (Supporting Information Figure S3). In all subjects, quantitative analysis of T_2 values was performed in three different ROIs: prostate peripheral zone (PZ), prostate central gland (CG), and obturator internus muscle; the results are presented as mean \pm STD using boxplots.

RESULTS

Simulations

The EPG-simulated magnetization evolution in time for the proposed acquisition scheme is shown in Figure 1b for two simulated prostate tissue types: cancerous ($T_2 = 50$ ms) and healthy ($T_2 = 150$ ms).

T_1 and FA dependence

The dependence of the magnetization signal extracted from the simulated dictionary on T_1 and FA are shown in Figure 2. While the signal intensity was more than a factor of 2.5 different for $T_2 = 50$ ms vs $T_2 = 150$ ms, which underlines the desired T_2 sensitivity of the proposed scheme, the signal intensity experienced only slight variations over a range of T_1 typically observed in the prostate (Figure 2a) and FA (Figure 2b). Specific simulations showed that the dictionary-based matching is robust to T_1 variations when $T_2^{\text{true}} = 50$ ms, for both $T_1^{\text{true}} = 1700$ and 2200 ms (light blue curves in Figure 3a and 3b), over a wide range of (wrongly) assumed T_1 values (1500-2400 ms). For $T_2^{\text{true}} = 150$ ms (dark blue curves in Figure 3a and 3b) the T_2 estimates experienced slight under- and overestimation when the (wrongly) assumed T_1 was respectively lower and higher than T_1^{true} (maximum absolute bias: 3% when $T_1^{\text{true}} = 1700$, 2% when $T_1^{\text{true}} = 2200$). This warrants that a global fixed T_1 and FA can be used in the dictionary matching for in vivo data.

SNR analysis

The SNR analysis results are presented in Figure 4. For illustration purposes, Figure 4a shows a dictionary entry with 100 corresponding random noise added signals as an example case of SNR analysis for SNR = 10. Figure 4b summarizes the SNR analysis simulation, showing accuracy and precision for the $T_2^{\text{low/high}} = 50/150$ ms, $T_1 = 2200$ ms tissue, for all the T_2 mapping methods under investigation. The monoexponential fit led to the lowest accuracy among all the scenarios analyzed, with a bias of 19.7 ms ($T_2^{\text{true}} - T_2^{\text{estimated}}$) and precision of 21 ms (STD) in the most challenging case of T_2^{high} at the lowest SNR (SNR = 10). The accuracy increased when using the dictionary-based T_2 matching, with very similar results when using six or three T_2^{prep} durations. In particular, the proposed method using only three T_2^{prep} modules led to a maximum bias of -0.4 ms in the T_2^{high} case at the lowest SNR, and a STD of 15.4 ms. For a more realistic SNR level (SNR = 30) the proposed T_2 mapping approach showed a maximum bias of -0.01 and -

0.16 ms for the T_2^{low} and T_2^{high} case respectively, and a corresponding STD of 1.99 and 5.04 ms. Overall, as expected, accuracy and precision increased at higher SNR and lower T_2 values.

Phantom

Results of T_2 mapping in the phantom are shown in Figure 5. Figure 5b shows the comparison of the T_2 estimates obtained with the FS 3D $T_2\text{prep}$ -bSSFP using both a simple monoexponential fit and the proposed dictionary-based matching compared with the gold standard 2D SE method. This analysis was performed for the four tubes highlighted in Figure 5a, so as to represent different combinations of T_1 and T_2 values. In concordance with our simulation results, the phantom data confirmed that the use of the simple monoexponential fit with the $T_2\text{prep}$ -bSSFP acquisition provided T_2 estimates that are significantly different ($P < 0.05$) from those obtained with the gold standard approach, whereas the T_2 values obtained with the dictionary approach were highly correlated (correlation of $r = 0.99$) with the gold standard T_2 values (Figure 5b). The tube with the highest T_1 and T_2 values (HH) was characterized by the lowest accuracy and precision. The use of the three-fold accelerated acquisition resulted in a scan time reduction from a FS TA = 8 min (100 shots per 3D acquisition x three $T_2\text{prep}$) to VD TA = 3 min (37 shots per 3D acquisition x three $T_2\text{prep}$). Results obtained with the VD $T_2\text{prep}$ -bSSFP were highly correlated with the FS acquisition results for all phantom tubes ($r = 0.99$, Figure 6a). Figure 6b shows the final comparison between the gold standard method (2D SE using monoexponential fit, TA = 1 h 56 min) and the proposed 3D VD $T_2\text{prep}$ -bSSFP dictionary-based matching using three $T_2\text{prep}$ (TA = 3 min), which were highly correlated ($r = 0.99$) over a range of T_1 and T_2 values ($T_1 = [250, \dots, 1900]$ ms, $T_2 = [50, \dots, 250]$ ms).

Healthy subjects

$T_2\text{w}$ images obtained with the VD 3D $T_2\text{prep}$ -bSSFP sequence at different $T_2\text{prep}$ durations and the corresponding dictionary-based $T_2\text{map}$ are shown in Figure 7 for three healthy subjects. T_2 estimates obtained with the proposed VD $T_2\text{prep}$ -bSSFP sequence in the PZ, CG and muscle for all healthy subjects are 97 ± 14 ms, 76 ± 7 ms, and 36 ± 3 ms respectively, as reported in Figure 8a. Overall, these values are lower compared to those typically found in the literature^{11,24,44}, except for one case with T_2 comparable to literature values (Figure 8c), which corresponds to the oldest subject in the cohort (age 37). An example case of a healthy subject with increased T_2 due to focal inflammation is presented

in Figure 9. An example image of the reference clinical standard 2D T₂w TSE and a comparison with the VD 3D T₂w T₂prep-bSSFP for the prostate area is shown in Supporting Information Figure S2. The ROI analysis performed on the T₂ map obtained for one subject nine months after the first scan, illustrated in Figure 10 (scan 1 vs. scan 2), shows good in-vivo scan reproducibility of the proposed approach. Indeed, all the estimated T₂ values in the second repeat are within one standard deviation of the first measurement. Specifically, the estimated mean \pm standard deviation T₂ values in scan 1 / scan 2 are: 89.7 \pm 5.4 / 93.1 \pm 5.7 ms in PZ, 72.0 \pm 7.2 / 73.3 \pm 5.4 ms in CG, and 37.7 \pm 5.5 / 38.9 \pm 2.7 ms in the muscle.

DISCUSSION

We have demonstrated the feasibility of using an accelerated 3D T₂-prepared multi-shot-bSSFP sequence combined with a dictionary-based matching method to rapidly quantify T₂ values in the prostate. The proposed method enabled the acquisition of a 3D T₂w image of the full pelvis FOV at 0.9 x 0.9 x 3 mm³ resolution in only 1 min, similar to that obtained in ²⁴ with a DESS sequence. The advantage of the proposed segmented acquisition in combination with dictionary based simulation of the acquisition-specific magnetization evolution lies in its flexibility to incorporate other magnetization preparation modules, e.g. diffusion preparation, T₁ preparation, fat suppression, and/or motion correction. Interleaved acquisitions, where multiple MR contrasts could be generated at each segment of the sequence, provide the prospect of an mpMRI approach that would enable a full tissue characterization with multiple and inherently co-registered quantitative maps in a single acquisition.

Recently proposed Magnetic Resonance Fingerprinting (MRF) relies on acquiring and analyzing pseudo-randomly encoded signals. The implementation of MRF requires specialized pulse sequences (for pseudo-random signal acquisitions) and custom image reconstruction code to generate the quantitative maps. The reconstruction of the severely undersampled MRF magnitude images is computationally demanding, and is therefore usually performed offline. On the contrary, our approach directly provides weighted images at different contrast weightings. Thus, clinicians can immediately evaluate image quality on T₂w scans. MRF still has some technical challenges, such as how long to sample the pseudo-random signal, the optimal choice of specific sequence parameters to be used, and the behaviour in presence of motion.

For our approach, the analysis of T_1 variation effects showed that small T_1 variations (in the range of T_1 values typically found within the prostate) do not affect the T_2 estimate significantly, providing the rationale for using a fixed T_1 value in our in-vivo study. When using a simulated T_1 value different from the true T_1 , high T_2 values (150 ms) estimated with the proposed mapping approach slightly deviate from the simulated T_2 , whereas the estimates seem to be very robust for low T_2 (50 ms). This might be related to the maximum T_2 prep duration used, which was 150 ms in this study. Our findings in the SNR analysis showed robustness of the proposed approach to different noise levels, with results comparable to those obtained in other studies ²⁰.

The main strength of simulation-based T_2 mapping is that it accounts for the magnetization evolution specific for the chosen acquisition sequence that cannot be accounted for when using the oversimplified monoexponential model. The reason why the standard monoexponential model is not suitable with our sequence is that the TR used, which was reduced to enable rapid scanning, does not allow for complete magnetization recovery (TR = 1600 ms, T_1 of the prostate ~ 2000 ms). Moreover, the monoexponential fitting does not accurately describe all the other parameters and effects occurring in the true sequence evolution, such as trajectory, T_1/T_2 ratio in the bSSFP readout, shot length, number of ramp-up pulses, number of segments. Indeed, our findings in simulations and phantom experiments consistently showed that acquisition-specific dictionary-based matching was able to obtain accurate T_2 estimates, while those obtained with the standard monoexponential fit showed significant deviation.

In the phantom study, we could acquire a long (TA = 1 h 56 min) SE scan as gold standard to evaluate bias and precision of our method. However, there is no gold standard for T_2 mapping in prostate imaging; different studies ^{20,24,44,47} used echo train sequences ⁴⁸ but these have been shown to lead to inaccurate estimates ²¹.

Our in-vivo T_2 values were lower than typical prostate T_2 values reported in the literature ^{11,24,44} which is likely due to biologically different prostate tissue due to the young age of our study population (aged 26 ± 6 years). This assumption is supported 1) as our measurements of T_2 in muscle was in agreement with values reported in the literature ²⁴, and 2) as our measurements of T_2 from the oldest subject of the cohort (37 years) were closer to literature values.

A limitation of this study is the presence of banding artifacts in the T_2 w images due to the use of a bSSFP readout. However, the prostate area was not affected by these artifacts and, if present, they were mainly seen in the region of fat. While bSSFP yields

the highest SNR efficiency, alternative methods with no or little banding artefacts include the non fully-balanced (SSFP, DESS) or spoiled (GRE, FLASH) readout acquisition, which could be used instead.

CONCLUSION

We have shown that rapid 3D T_2 -mapping of the prostate is feasible in 3 min using an accelerated 3D multi shot T_2 -prepared acquisition combined with a dictionary-based T_2 mapping reconstruction. Our proposed approach showed high precision and accuracy for T_2 quantification and allows for a flexible incorporation of additional magnetization preparation modules to be used in an mpMRI protocol for PCa detection and characterization.

ACKNOWLEDGEMENTS

This work was supported by the King's College London & Imperial College London EPSRC Centre for Doctoral Training in Medical Imaging [EP/L015226/1]; the Wellcome EPSRC Centre for Medical Engineering at King's College London [WT 203148/Z/16/Z]; the King's Health Partners Research and Development Challenge Fund; TOHETI; NIHR BRC; GSTT/KCL BRC; CRUK/EPSRC Cancer Centre; Siemens Healthineers.

REFERENCES

1. WHO. GLOBOCAN 2012: Estimated Incidence, Mortality and Prevalence Worldwide in 2012. http://globocan.iarc.fr/Pages/fact_sheets_cancer.aspx. Published 2012. Accessed March 15, 2018.
2. Cancer Research UK: Prostate Cancer Statistics. <http://www.cancerresearchuk.org/health-professional/cancer-statistics/statistics-by-cancer-type/prostate-cancer>. Accessed April 9, 2017.
3. National Cancer Institute. Cancer Stat Facts: Prostate Cancer. <https://seer.cancer.gov/statfacts/html/prost.html>. Published 2018. Accessed July 20, 2018.
4. Hegde J V., Mulkern R V., Panych LP, et al. Multiparametric MRI of prostate cancer: An update on state-of-the-art techniques and their performance in detecting and localizing prostate cancer. *J Magn Reson Imaging*. 2013;37(5):1035-1054. doi:10.1002/jmri.23860.
5. Barentsz JO, Richenberg J, Clements R, et al. ESUR prostate MR guidelines 2012. *Eur Radiol*. 2012;22(4):746-757. doi:10.1007/s00330-011-2377-y.
6. Ahmed HU, El-Shater Bosaily A, Brown LC, et al. Diagnostic accuracy of multiparametric MRI and TRUS biopsy in prostate cancer (PROMIS): a paired validating confirmatory study. *Lancet*. 2017;6736(16):1-8. doi:10.1016/S0140-6736(16)32401-1.
7. Weinreb JC, Barentsz JO, Choyke PL, et al. PI-RADS Prostate Imaging - Reporting and Data System: 2015, Version 2. *Eur Urol*. 2016;69(1):16-40. doi:10.1016/j.eururo.2015.08.052.
8. Isebaert S, Van Den Bergh L, Haustermans K, et al. Multiparametric MRI for prostate cancer localization in correlation to whole-mount histopathology. *J Magn Reson Imaging*. 2013;37(6):1392-1401. doi:10.1002/jmri.23938.
9. Le JD, Tan N, Shkolyar E, et al. Multifocality and prostate cancer detection by multiparametric magnetic resonance imaging: Correlation with whole-mount histopathology. *Eur Urol*. 2015;67(3):569-576. doi:10.1016/j.eururo.2014.08.079.
10. Liu W, Turkbey B, Senegas J, et al. Accelerated T2 mapping for characterization of prostate cancer. *Magn Reson Med*. 2011;65(5):1400-1406. doi:10.1002/mrm.22874.

11. Yamauchi FI, Penzkofer T, Fedorov A, et al. Prostate Cancer Discrimination in the Peripheral Zone With a Reduced Field-of-View T2 -mapping MRI Sequence. *Magn Reson Imaging*. 2015;33(5):525-530. doi:10.1002/aur.1474.Replication.
12. Roebuck JR, Haker SJ, Mitsouras D, Rybicki FJ, Tempny CM, Mulkern R V. Carr-Purcell-Meiboom-Gill (CPMG) Imaging of Prostate Cancer: Quantitative T2 Values for Cancer Discrimination. *Magn Reson Imaging*. 2009;27(4):497-502. doi:10.3816/CLM.2009.n.003.Novel.
13. van Houdt PJ, Agarwal HK, van Buuren LD, et al. Performance of a fast and high-resolution multi-echo spin-echo sequence for prostate T2 mapping across multiple systems. *Magn Reson Med*. 2017;00(January):1-9. doi:10.1002/mrm.26816.
14. Liney GP, Turnbull LW, Lowry M, Turnbull LS, Knowles AJ, Horsman A. In vivo quantification of citrate concentration and water T2 relaxation time of the pathologic prostate gland using H1 MRS and MRI. *Magn Reson Imaging*. 1997;15(10):1177-1186.
15. Agarwal HK, Senegas J, Turkbey B, et al. Whole-Prostate T2 mapping in under 6 minutes using autocalibration and partial-fourier MRI. *Proc Intl Soc Mag Reson Med*. 2012;20:2401.
16. Lee D, Jin KH, Kim EY, Park SH, Ye JC. Acceleration of MR parameter mapping using annihilating filter-based low rank hankel matrix (ALOHA). *Magn Reson Med*. 2016;76(6):1848-1864. doi:10.1002/mrm.26081.
17. Zhao B, Wenmiao L, Hitchens K, Lam F, Ho C, Liang Z-P. Accelerated MR Parameter Mapping with Low-Rank and Sparsity Constraints. *Magn Reson Med*. 2015:489-498. doi:10.1002/aur.1474.Replication.
18. Peng X, Ying L, Liu Y, Yuan J, Liu X, Liang D. Accelerated exponential parameterization of T2 relaxation with model-driven low rank and sparsity priors (MORASA). *Magn Reson Med*. 2016;00(November 2015). doi:10.1002/mrm.26083.
19. Doneva M, Boernert P, Eggers H, Stehning C, S??n??gas J, Mertins A. Compressed sensing reconstruction for magnetic resonance parameter mapping. *Magn Reson Med*. 2010;64(4):1114-1120. doi:10.1002/mrm.22483.
20. Ben-Eliezer N, Sodickson DK, Block KT. Rapid and accurate T2 mapping from multi-spin-echo data using bloch-simulation-based reconstruction. *Magn Reson Med*. 2015;73(2):809-817. doi:10.1002/mrm.25156.
21. Hennig J. Multiecho imaging sequences with low refocusing flip angles. *J Magn*

- Reson.* 1988;78(3):397–407.
22. Weigel M. Extended phase graphs: Dephasing, RF pulses, and echoes - Pure and simple. *J Magn Reson Imaging.* 2015;41(2):266-295. doi:10.1002/jmri.24619.
 23. Stöcker T, Keil F, Vahedipour K, Brenner D, Pracht E, Shah NJ. MR parameter quantification with magnetization-prepared double echo steady-state (MP-DESS). *Magn Reson Med.* 2014;72(1):103-111. doi:10.1002/mrm.24901.
 24. Dregely I, Margolis DAJ, Sung K, et al. Rapid quantitative T2 mapping of the prostate using three-dimensional dual echo steady state MRI at 3T. *Magn Reson Med.* 2016;76(6):1720-1729. doi:10.1002/mrm.26053.
 25. Heule R, Ganter C, Bieri O. Triple echo steady-state (TESS) relaxometry. *Magn Reson Med.* 2014;71(1):230-237. doi:10.1002/mrm.24659.
 26. Akcakaya M, Weingartner S, Basha TA, Roujol S, Bellm S, Nezafat R. Joint myocardial T1 and T2 mapping using a combination of saturation recovery and T2-preparation. *Magn Reson Med.* 2016;76(3):888-896. doi:10.1002/mrm.25975.
 27. Aliotta E, Moulin K, Zhang Z, Ennis DB. Simultaneous measurement of T2 and apparent diffusion coefficient (T2 +ADC) in the heart with motion-compensated spin echo diffusion-weighted imaging. *Magn Reson Med.* 2017;00(March):1-9. doi:10.1002/mrm.26705.
 28. Santini F, Kawel-Boehm N, Greiser A, Bremerich J, Bieri O. Simultaneous T1 and T2 quantification of the myocardium using cardiac balanced-SSFP inversion recovery with interleaved sampling acquisition (CABIRIA). *Magn Reson Med.* 2015;74(2):365-371. doi:10.1002/mrm.25402.
 29. Giri S, Chung Y-C, Merchant A, et al. T2 quantification for improved detection of myocardial edema. *J Cardiovasc Magn Reson.* 2009;11(1):56. doi:10.1186/1532-429X-11-56.
 30. Van Heeswijk RB, Feliciano H, Bongard C, et al. Free-breathing 3 T magnetic resonance T2-mapping of the heart. *JACC Cardiovasc Imaging.* 2012;5(12):1231-1239. doi:10.1016/j.jcmg.2012.06.010.
 31. Tourais J, Henningsson M, Botnar R. Free-breathing 3D myocardial T2 mapping using image-based respiratory motion correction. In: *International Society for Magnetic Resonance in Medicine (ISMRM).* ; 2016.
 32. Nguyen C, Sharif-Afshar AR, Fan Z, et al. 3D high-resolution diffusion-weighted MRI at 3T: Preliminary application in prostate cancer patients undergoing active surveillance protocol for low-risk prostate cancer. *Magn Reson Med.*

- 2016;75(2):616-626. doi:10.1002/mrm.25609.
33. Dregely I, Prieto C, Neji R, et al. " Push-button " PET / MRI using a continuous scan 3D quantitative T2 MRI sequence. *Proc Intl Soc Mag Reson Med*. 2017;1239:2078.
 34. Shankar R, Cruz G, Neji R, et al. Accelerated 3D T2-Mapping of the Prostate in 3.5 min using TV-SENSE Reconstruction. In: *ESMRMB*. ; 2017:139.
 35. Kellman P, Hansen MS. T1-mapping in the heart: Accuracy and precision. *J Cardiovasc Magn Reson*. 2014;16(1):1-20. doi:10.1186/1532-429X-16-2.
 36. Brittain JH, Hu BS, Wright GA, Meyer CH, Macovski A, Nishimura DG. Coronary Angiography with Magnetization-Prepared T2 Contrast. *Magn Reson Med*. 1995;33(5):689-696. doi:10.1002/mrm.1910330515.
 37. Botnar RM, Stuber M, Danias PG, Kissinger K V, Manning WJ. Improved Coronary Artery Definition With T2-Weighted, Free-Breathing, Three-Dimensional Coronary MRA. *Circulation*. 1999;99(24):3139-3148. doi:10.1161/01.CIR.99.24.3139.
 38. Prieto C, Doneva M, Usman M, et al. Highly efficient respiratory motion compensated free-breathing coronary MRA using golden-step Cartesian acquisition. *J Magn Reson Imaging*. 2015;41(3):738-746. doi:10.1002/jmri.24602.
 39. Deshpande VS, Chung Y-C, Zhang Q, Shea SM, Li D. Reduction of Transient Signal Oscillations in True-FISP Using a Linear Flip Angle Series Magnetization Preparation. *Magn Reson Med*. 2003;49:151-157. doi:10.1002/mrm.10337.
 40. Cruz G, Atkinson D, Buerger C, Schaeffter T, Prieto C. Accelerated motion corrected three-dimensional abdominal MRI using total variation regularized SENSE reconstruction. *Magn Reson Med*. 2016;75(4):1484-1498. doi:10.1002/mrm.25708.
 41. Lustig M, Donoho DL, Santos JM, Pauly JM. Compressed sensing MRI. *IEEE Signal Process Mag*. 2008;25(March 2008):72-82. doi:Doi 10.1109/Tit.2006.871582.
 42. Gibbs P, Liney GP, Pickles MD, Zelhof B, Rodrigues G, Turnbull LW. Correlation of ADC and T2 measurements with cell density in prostate cancer at 3.0 Tesla. *Invest Radiol*. 2009;44(9):572-576. doi:10.1097/RLI.0b013e3181b4c10e.
 43. Sabouri S, Chang SD, Savdie R, et al. Luminal Water Imaging: A New MR Imaging T2 Mapping Technique for Prostate Cancer Diagnosis. *Radiology*. 2017;284(2):161687. doi:10.1148/radiol.2017161687.

44. Liu W, Turkbey B, Senegas J, et al. Accelerated T2 mapping for characterization of prostate cancer. *Magn Reson Med*. 2011;65(5):1400-1406. doi:10.1002/mrm.22874.
45. Rangwala NA, Dregely I, Wu HH, Sung K. Optimization and evaluation of reference region variable flip angle (RR-VFA) B1+ and T1 Mapping in the Prostate at 3T. *J Magn Reson Imaging*. 2017;45(3):751-760. doi:10.1002/jmri.25410.
46. Captur G, Gatehouse P, Kellman P, et al. A T1 and ECV phantom for global T1 mapping quality assurance: The T1 mapping and ECV standardisation in CMR (T1MES) program. *J Cardiovasc Magn Reson*. 2016;18(1):W14. doi:10.1186/1532-429X-18-S1-W14.
47. de Bazelaire CM, Duhamel GD, Rofsky NM, Alsop DC. MR imaging relaxation times of abdominal and pelvic tissues measured in vivo at 3.0 T: Preliminary results. *Radiology*. 2004;230(3):652-659. doi:10.1148/radiol.2303021331.
48. Hilbert T, Sumpf TJ, Weiland E, et al. Accelerated T₂ mapping combining parallel MRI and model-based reconstruction: GRAPPATINI. *J Magn Reson Imaging*. 2018:1-10. doi:10.1002/jmri.25972.

FIGURE LEGENDS

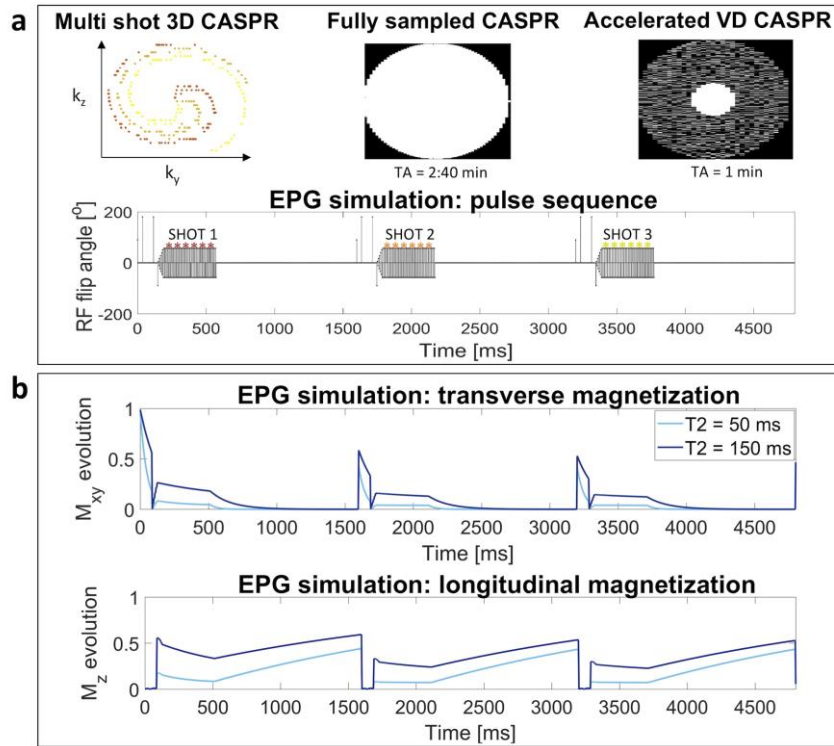


Figure 1: (a) Multi shot 3D CASPR trajectory with fully sampled and variable density masks, shown together with three shots of the 3D multi-shot T₂prep-bSSFP pulse sequence. (b) Corresponding transverse and longitudinal magnetization evolution obtained using the EPG simulation framework, for two different simulated T₂ values (50 and 150 ms). Other parameters of the simulation were: T₁ = 2200 ms, TR = 1600 ms, FA = 57°, T₂prep duration = 90 ms.

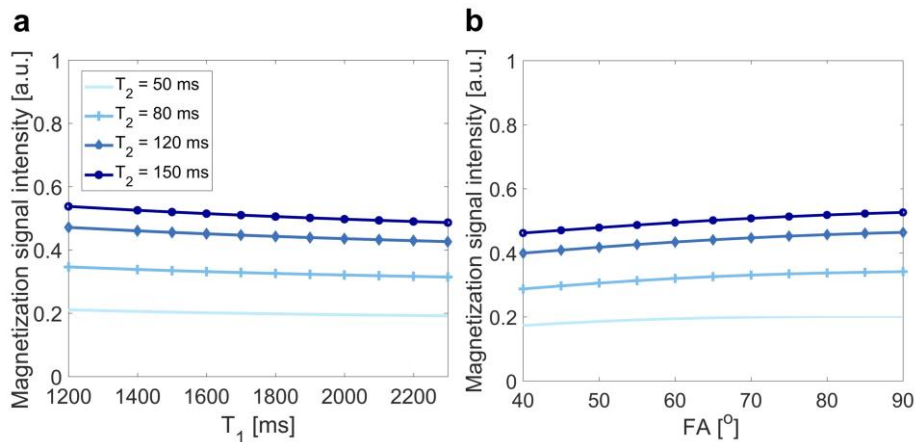


Figure 2: Insensitivity of the simulated signal intensity to T₁ variations typically observed in the prostate (a) and flip angle (FA) (b), for T₂ = 50, 80, 120, 150 ms. Other sequence parameters are: TR = 1600 ms, FA = 57° (a), T₁ = 2200 ms (b).

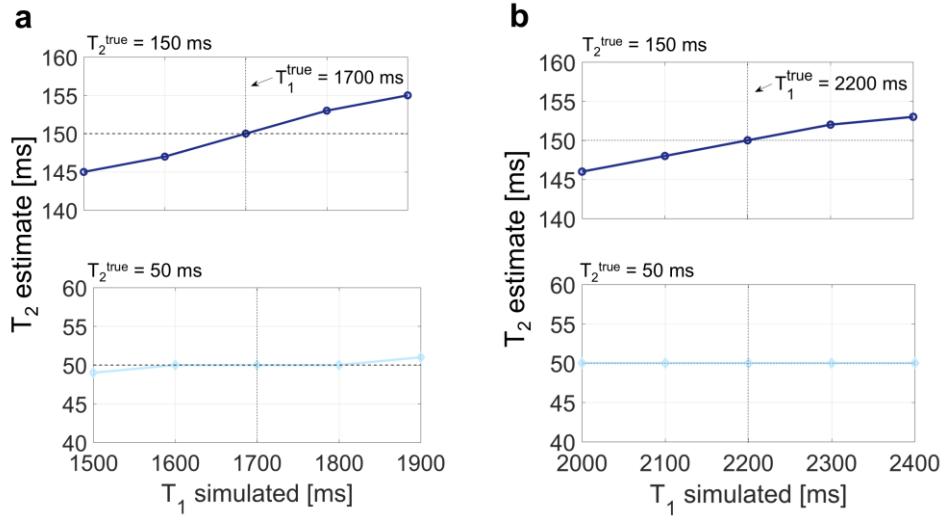


Figure 3: Simulation of the effect of using a T_1 value that differs from the T_1^{true} on the proposed dictionary-based T_2 mapping method, for different simulated tissue types. (a) $T_1^{\text{true}} = 1700$ ms, $T_2^{\text{true}} = 50$ and 150 ms. (b) $T_1^{\text{true}} = 2200$ ms, $T_2^{\text{true}} = 50$ and 150 ms. The mapping seems to be very robust for low T_2 (50 ms), whereas higher T_2 (150 ms) values are slightly underestimated or overestimated when the simulated T_1 is respectively lower or higher than the T_1^{true} .

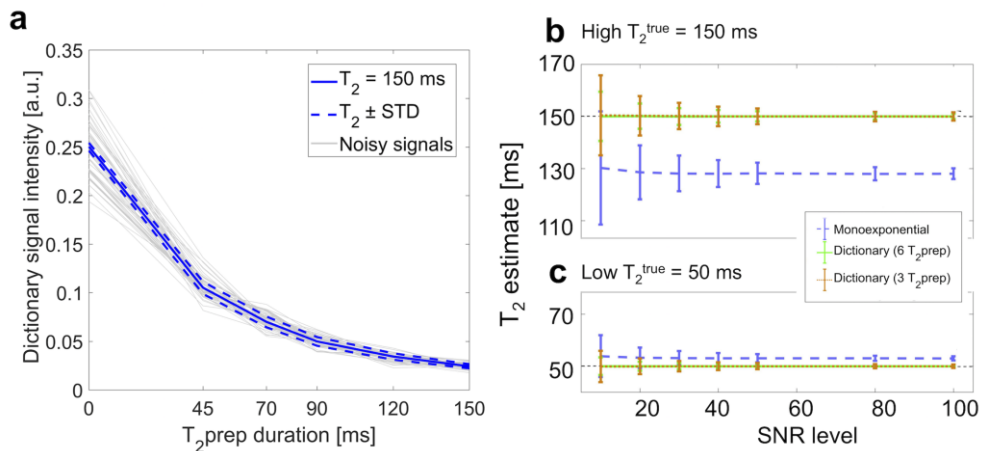


Figure 4: SNR analysis with different SNR levels, where accuracy and precision are calculated as the mean and standard deviation of the T_2 values estimated in the 5000 iterations of the Monte Carlo simulation, respectively. (a) Dictionary entry with corresponding 100 noisy signals overlapped as an example case of SNR analysis for SNR = 10. T_2 estimates for $T_2 = 150$ ms (b) and $T_2 = 50$ ms (c) for all three T_2 mapping methods: monoexponential fit and dictionary-based matching with six and three T_2 prep durations. The monoexponential fit led to a lower accuracy, showing a substantial bias, whereas with the dictionary-based matching the accuracy of the T_2 estimate improved, with estimates comparable to the true simulated values.

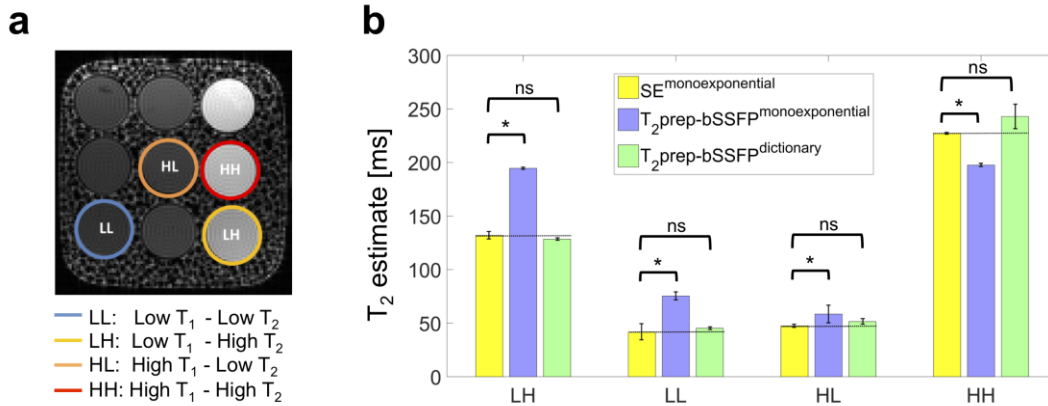


Figure 5: (a) 2D SE T₂w image of the phantom; four tubes with different T₁ and T₂ combinations are highlighted in different colors. (b) Comparison of T₂ values obtained in the phantom tubes highlighted in (a) with: gold standard 2D SE acquisition using monoexponential fit (yellow bar), fully sampled 3D T₂prep-bSSFP using both monoexponential fit (purple bar) and dictionary matching (green bar). Compared to gold standard, T₂ values obtained with the T₂prep-bSSFP using monoexponential fitting were significantly different (P < 0.05), whereas the acquisition-specific dictionary-based matching corrected for these inaccurate estimates.

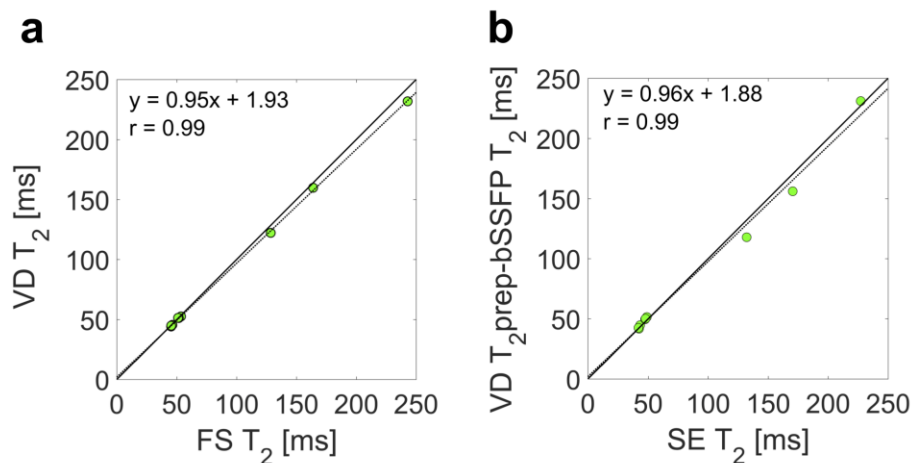


Figure 6: (a) Correlation plot of T₂ values in all 9 phantom tubes obtained with FS and VD 3D T₂prep-bSSFP acquisitions, both obtained with the proposed dictionary matching approach, showing a correlation value $r = 0.99$. (b) Correlation plot between gold standard 2D SE using monoexponential fit (TA = 1 h 56 min) and proposed rapid method (VD 3D T₂prep-bSSFP with dictionary matching using three T₂prep, TA = 3 min), with correlation value $r = 0.99$.

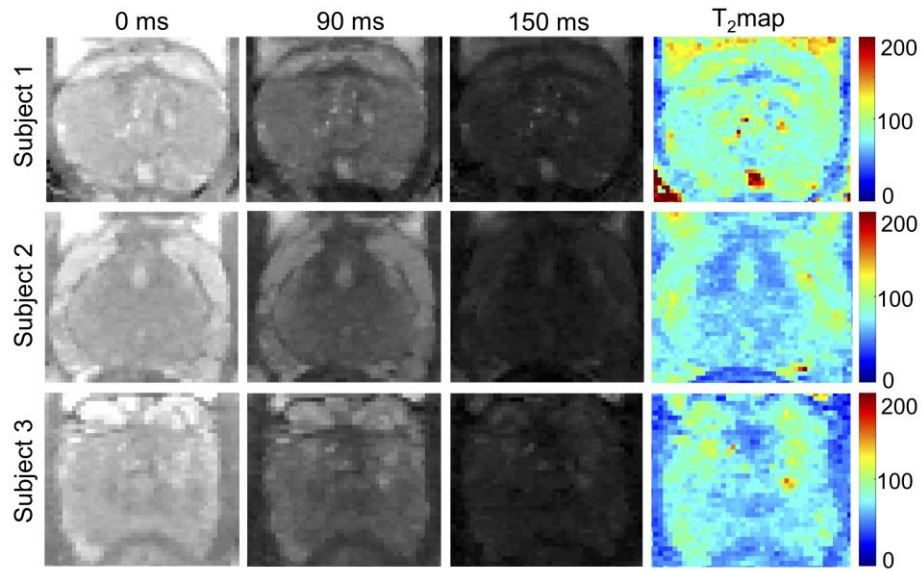


Figure 7: T₂w prostate images obtained with VD 3D T₂prep-bSSFP and three different T₂prep durations (0, 90, 150 ms), and corresponding T₂map obtained with the proposed dictionary-based T₂ mapping, for three representative healthy subjects.

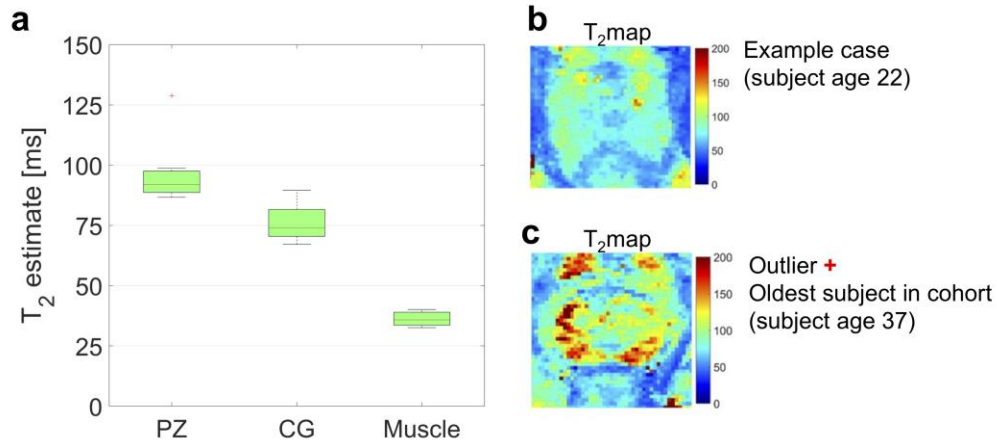


Figure 8: (a) T₂ values of peripheral zone (PZ), central gland (CG) and muscle in the healthy subjects obtained with the proposed VD 3D T₂prep-bSSFP sequence and dictionary-based T₂ mapping. Example cases of a typical T₂ map representative of our young subject population (age 26 ± 6) (b) and of one subject which is the oldest subject in the cohort (age 37) (c).

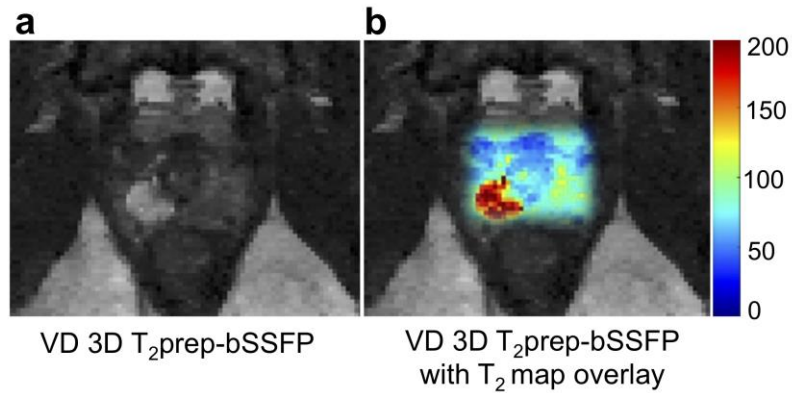


Figure 9: Example case of a healthy subject with focal inflammation found in the peripheral zone (PZ). (a) 3D VD T₂w T₂prep-bSSFP (T₂prep = 90 ms) with T₂ map overlay (b). Estimated T₂ values with the proposed 3D VD T₂prep-bSSFP using dictionary matching are T₂ = 89 ± 16 ms in the normal PZ and 188 ± 26 ms in the inflammation area.

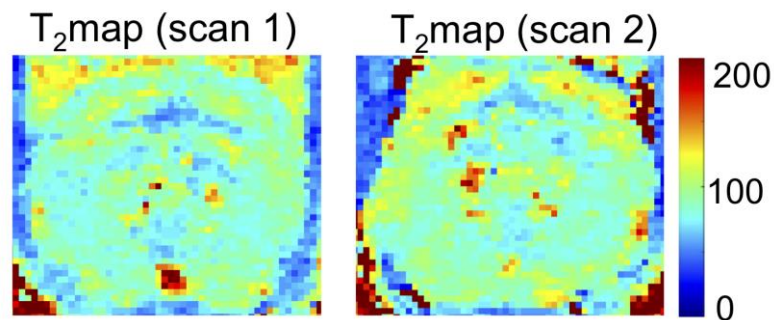
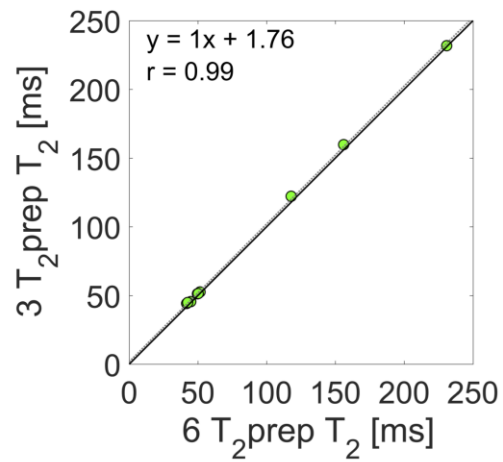
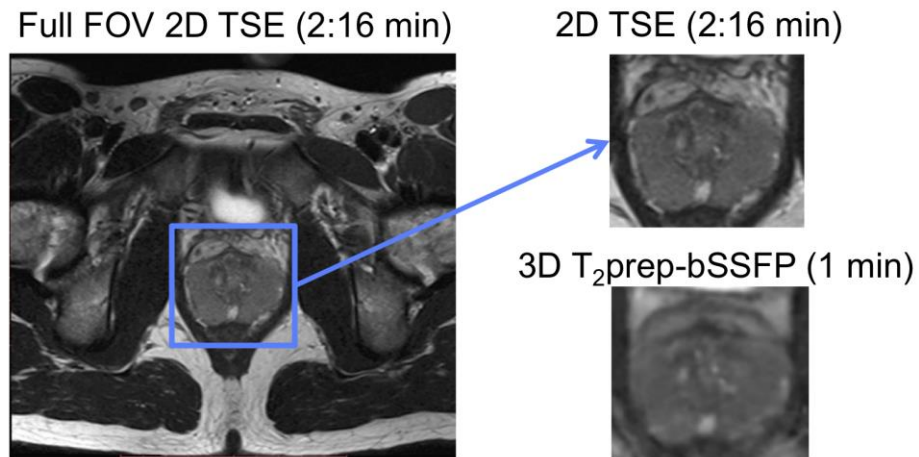


Figure 10: In-vivo scan reproducibility performed for one healthy subject acquiring three additional VD T₂prep-bSSFP T₂w images 9 months after the first scan. The T₂ map was performed again with the proposed dictionary matching, showing good reproducibility. Estimated mean T₂ values in scan 1 / scan 2 are: 89.7 ± 5.4 / 93.1 ± 5.7 ms in PZ, 72.0 ± 7.2 / 73.3 ± 5.4 ms in CG, and 37.7 ± 5.5 / 38.9 ± 2.7 ms in the muscle.

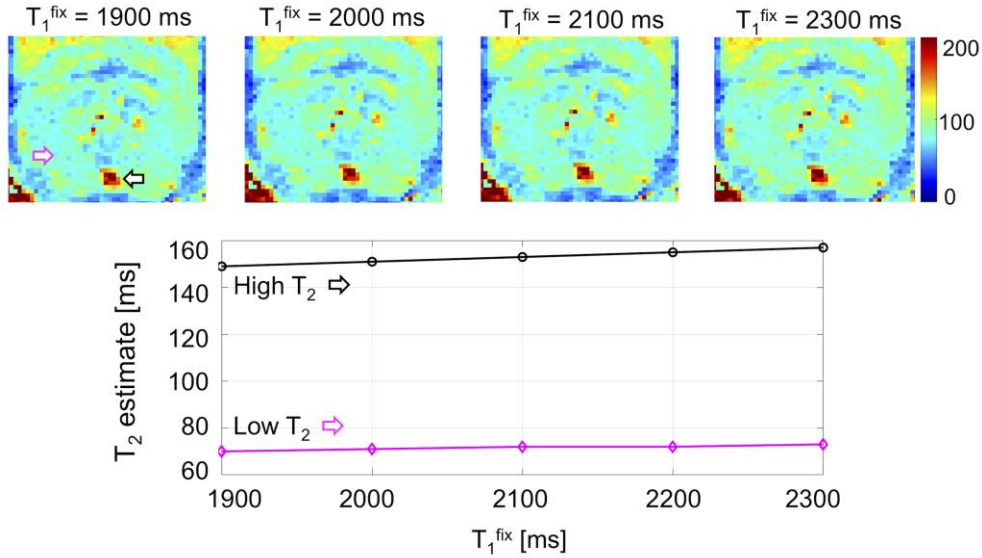
SUPPLEMENTARY FIGURE LEGENDS



Supporting Information Figure S1: Correlation plot of T_2 values obtained in the phantom with VD 3D $T_{2\text{prep}}$ -bSSFP acquisition with dictionary matching using six $T_{2\text{prep}}$ and three $T_{2\text{prep}}$, showing high correlation ($r = 0.99$). The scan time is reduced from $T_A = 6$ min to 3 min when using only three $T_{2\text{prep}}$.



Supporting Information Figure S2: Full field of view (FOV) of the reference clinical standard 2D T_{2w} TSE acquisition (resolution $0.6 \times 0.8 \times 3 \text{ mm}^3$, $TE = 89 \text{ ms}$) with detail of the prostate, together with the VD 3D T_{2w} $T_{2\text{prep}}$ -bSSFP image (resolution $0.9 \times 0.9 \times 3 \text{ mm}^3$, $T_{2\text{prep}}$ duration 90 ms).



Supporting Information Figure S3: Sensitivity experiment performed in-vivo to show the impact on the T_2 map estimated using the proposed dictionary matching approach with different assumed globally fixed T_1 values. The T_2 maps are shown for one healthy subject, where four different T_1 that deviates from the finally chosen T_1 value (2200 ms) were used in the dictionary matching. The plots at the bottom show the dependence of the T_2 estimate over the range of fixed T_1 used, for two different pixels characterized by low and high T_2 (indicated by magenta and black arrow respectively). The observed variation in T_2 estimate is within 4%, showing robustness to T_1 variations of the proposed mapping method, not only in simulations

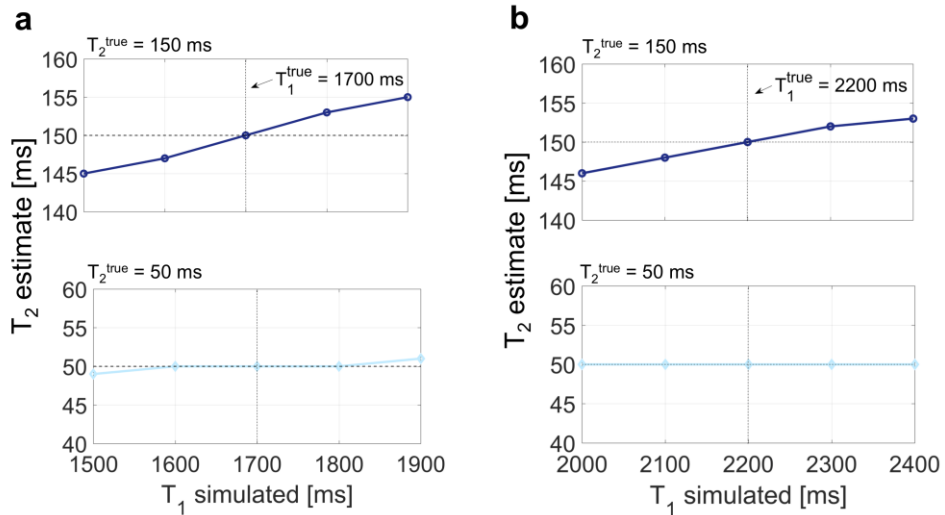


(Figure 2 and

Figure 3) but also in-vivo.